Scaling-up of an Insect Cell-based Virus Production Process in a Novel Single-use Bioreactor with Flexible Agitation

Stephan C. Kaiser[1],*, Paula N. Decaria[2], Stefan Seidel[3], and Dieter Eibl[3]

A novel single-use bioreactor was recently introduced to the market that is agitated by impellers suspended on flexible ropes rather than a rigid shaft. Computational fluid dynamics (CFD) models were created and validated by particle image velocimetry (PIV) to predict the bioreactor's fluid flow and mixing. The data were then used to scale-up a *Spodoptera frugiperda*, subclone 9 (Sf9) insect cell-based production of recombinant adeno-associated virus (AAV) from a benchtop glass bioreactor to the single-use system with 30 L working volume. This viral vector is one of the most commonly used in gene therapies. The volumetric power input was kept constant while maintaining reasonable mixing times and shear stresses between the scales. Peak cell densities of up to 7.2×10^6 cells mL^{-1} and maximum virus titers of 1.7×10^{11} vg mL^{-1} were achieved. Similar cell growth and metabolite profiles further proved the successful process transfer between the two geometrically non-similar bioreactor systems. The pilot bioreactor yielded between 3.3 and 4.8×10^{15} vg that, depending on the therapy, can be sufficient for the treatment of a single patient.

1 Introduction

In 2020, the world-wide market for insect cell expression systems was estimated to be $275 million, with the majority generated using subclone 9 (Sf9) and subclone 21 (Sf21) from the fall armyworm, *Spodoptera frugiperda*, as well as TN5B1-4 (Hi-5) cells from the cabbage looper, *Trichoplusia ni* [1]. The virus-like particles (VLP) produced by these insect cells are commonly outstandingly immunogenic and therefore potentially useful as vaccines, with some candidates being commercially available (e.g., the human papilloma virus vaccine Cervarix™) and others under development [2]. The Gibco™ ExpiSf system was the first-ever chemically defined baculovirus expression system that can utilize a non-engineered derivative of Sf9 insect cells, which have been adapted for high-density suspension growth, and a specialized vector for insect cells. While most Sf9 cultures have been conducted in low-hydrolysate media, such as Sf900III [3], established cultivation protocols for the chemically defined media were very limited, especially for scales beyond the single-digit liter range. Sf9 TriEx™ cells have been cultivated in the ExpiSf CDM media using shake flasks, and a higher cell viability compared with three other media was noticed [4]. Furthermore, it has been demonstrated that baculovirus-infected ExpiSf9 cells can produce up to 19-fold higher yields than those obtained from the

conventional Sf9 cell-based systems [5]. However, to the best of the author's knowledge, no large-scale AAV production with Sf9 cells using chemically defined media have been described in the literature.

The Thermo Scientific™ DynaDrive™ S.U.B. (Single-Use Bioreactor) uses a novel agitation concept based on impeller elements that are attached to two flexible ropes rather than a rigid shaft [6]. This design provides improved performance and scalability to larger volumes with enhanced mixing from the multi-stage impellers. The cuboidal tank shape and the off-centered drive train reduced the tangential flow avoiding vortex formation often seen in cylindrical vessels (data not published). In addition, the flexible and collapsi-

[1]Dr. Stephan C. Kaiser
(Stephan.Kaiser@thermofisher.com)
Thermo Scientific, BioProduction Group, Single-Use Technology, 3311 Leonard Court, CA-95054 Santa Clara, USA.

[2]Paula N. Decaria
Thermo Scientific, BioProduction Group, Single-Use Technology, 1325 N 1000 W, UT-84321 Logan, USA.

[3]Stefan Seidel, Prof. Dr. Dieter Eibl
ZHAW School of Life Sciences and Facility Management, Centre for Biochemical Engineering and Cell Cultivation Technique, Grüentalstrasse, CH-8810 Wädenswil, Switzerland.

ble design allows for a compact packaging for transport and storage [6]. Another advantage of the DynaDrive S.U.B. over other single-use systems is the high turn-down ratio of 10:1, increasing the flexibility and potentially avoiding intermediate steps during the seed train. Furthermore, the ergonomics of the existing DynaDrive S.U.B. series have been improved making loading and unloading of the bioprocess container (BPC) easier for the operator [7]. However, only limited data and knowledge about the hydrodynamics and mixing of this system were available. To help overcome this limitation, computational fluid dynamics (CFD) models were created to predict the fluid flow inside the DynaDrive S.U.B. using different working volumes. Similar studies have been published for other single-use bioreactors [8–10]. The present study aims for a scale-up approach for the ExpiSf9 baculovirus expression system from benchtop (2 L) to pilot scale (30 L working volume) based on the numerical models developed for the two geometrically non-similar bioreactor systems. The main goal was to transfer the insect cell culture process established at the bench-top scale to a pilot scale manufacturing of adeno-associated virus (AAV) material. Furthermore, the feasibility of the recently introduced DynaDrive S.U.B. for insect cell cultures should be demonstrated.

2 Material and Methods

2.1 Bioreactors

The benchtop-scale Thermo Scientific™ HyPerforma™ 3 L Glass bioreactor, which had been used previously for internal *Sf-9* insect cell process development studies [11], and the DynaDrive 50 L S.U.B. were used for the investigations. The cylindrical glass bioreactor with a diameter of 130 mm has a dished bottom, and it was agitated by two impellers, a modified Rushton turbine and a segment blade impeller, with diameters of 56 mm. More geometrical details are given in Tab. 1.

The DynaDrive 50 L S.U.B. consists of a cuboidal BPC made from Thermo Scientific™ Aegis™ 5-14 film that is mounted in a stainless-steel bag holder. Its agitation system consists of a drive train made up of three marine impellers with diameters of 132 mm that are strategically scaling a flexible rope ladder, as well as a sweep impeller at the base of the ladder. The BPC had a dual-sparger design with enhanced drilled-hole sparger (DHS) and porous-frit sparger, but only the DHS was used for aeration in this study. More information can be found in the product brochure [12] and data sheet [13] provided by the manufacturer. The bags were gamma-irradiated at 25–40 kGy. Sterilizable 12 mm probes for dissolved oxygen (Hamilton, VisiFerm ODO) and pH (Hamilton, EasyFerm Plus) measurements were used in both bioreactors. Thermo Scientific™ G3Pro™ and G3Lab™ Bioprocess Controllers and TruBio™ Bioprocess

Table 1. Summary of geometrical details of the two bioreactor systems used in this study.

	HyPerforma™ 3 L Glass Bioreactor	DynaDrive™ 50 L S.U.B.
Vessel/bag shape	Cylindrical	Cuboidal
Vessel/bag dimensions [mm]	130 (D)	253×265 (W×L)
Vessel/bag height [mm]	250	1020
Filling height [mm]	155	740
Max. working volume [L]	2	50
Impellers	Modified Rushton turbine (1) & segment blade impeller (1)	Marine impeller (3) & swept impeller (1)
Impeller diameter [mm]	56	132
Off-bottom clearance[a] [mm]	49	113
Impeller clearance[b] [mm]	64	356
Sparger	DHS	DHS & porous frit
Hole diameter [mm]	0.8	0.08 & 0.02–0.04
Number of holes	8	1448 & N/A
Temperature control	Silicone heater, 110 W	Water filled double-jacket with external TCU (1.2 kW)
Online measurements	Dissolved oxygen (Hamilton VisiFerm ODO), pH value (Hamilton EasyFerm Plus), temperature (Omega Pt100 RTD)	

[a] The off-bottom clearance is measured from the bioreactor bottom to the mid-plane of the lowest impeller, [b] The impeller clearance is measured as the distance between the two impeller mid-planes.

Control Software (v5.0) powered by the Emerson™ DeltaV™ (v13.0) Distributed Control Platform were used for data acquisition and control.

2.2 Computational Fluid Dynamics

CFD models of the two bioreactors used in this study were developed in the commercial ANSYS Fluent CFD package (v19.0, ANSYS workbench). Using the integrated meshing tool, the fluid domains for the different filling volumes were discretized by unstructured, body-fitted meshes (Fig. 1). While the characteristic length scales were kept constant for both volumes in each system, it was not possible to maintain the same resolution for the benchtop and pilot scale systems at a reasonable computational cost. The mesh characteristics are summarized in Tab. 2. Grid independent results were obtained for both systems (data not shown). The volumes were split into two zones (marked in grey in Fig. 1) in order to use the multiple reference frame (MRF) methodology for the steady state simulations. The two-equation realizable k–ε turbulence model was used to solve the Reynolds averaged Navier-Stokes equations [14]. First-order upwind schemes in conjunction with the least-square cell-based algorithm were used to solve the discretized conservation equations. All walls were treated with non-slip boundary conditions and constant fluid properties (density 993.3 kg m^{-3} and viscosity 0.6913 mPa s) were assumed for the single-phase simulations.

The agitator's volumetric power input (P/V_L) was estimated based on the torque (M) on the agitator, the shaft and, in case of the DynaDrive bioreactor, the agitator rope, as given by Eq. (1),

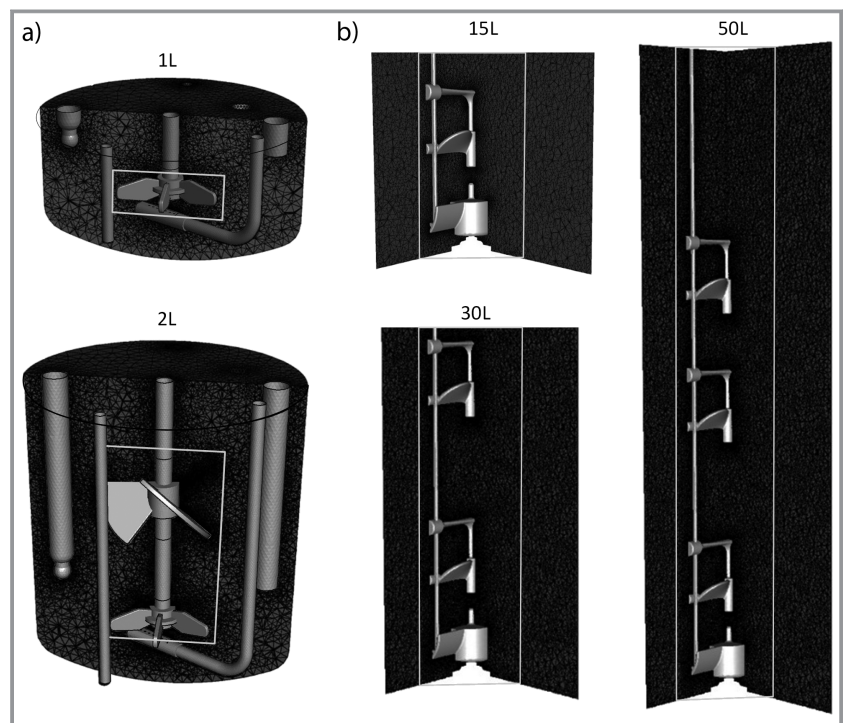$$P/V_L = \frac{2\pi N_R \sum M_i}{V_L} \qquad (1)$$

Figure 1. Meshes of the fluid domains of the a) glass bioreactor and b) DynaDrive S.U.B. The grey frames indicate the inner moving zone for the MRF model.

where N_R is the rotational speed and V_L is the liquid volume. The power number P_0 was then calculated from Eq. (2) where ρ_L is the density of the liquid and d_R is the impeller diameter.

$$P_0 = \frac{P}{\rho_L \, N_R^3 \, d_R^5} \qquad (2)$$

The mixing time was calculated based on the tracer method by solving an additional mass balance equation for an inert tracer. The time-dependent tracer concentration was simulated at a fixed time step size of 0.001 s, and the mixing time was defined as the duration required to achieve 95 % homogeneity. The hydrodynamic stresses τ_i were expressed by velocity gradients in flow direction (normal gradients $\dot{\gamma}_{nn}$) and by gradients perpendicular to the flow direction

Table 2. Summary of mesh details of the two bioreactor systems.

	HyPerforma™ 3-L glass bioreactor		DynaDrive™ 50-L single-use bioreactor		
	1 L	2 L	15 L	30 L	50 L
Mesh size	1 472 425	2 675 047	985 911	2 347 407	3 260 288
Elements in rotating zone	883 455	1 605 028	739 433	1 760 555	2 445 216
Elements in stationary zone	588 970	1 070 019	246 478	586 852	815 072
Max. skewness	0.91	0.91	0.92	0.92	0.93
Min. orthogonality	0.151	0.153	0.157	0.158	0.152

(shear gradients $\dot{\gamma}_{nt}$). As previously proposed [15], the individual velocity gradients were calculated as follows:

$$\tau_{nn} = \mu_L\, \dot{\gamma}_{nn} = \mu_L \sqrt{2\left(\frac{\partial \tilde{u}_x}{\partial \tilde{x}}\right)} \tag{3}$$

$$\tau_{nt} = \mu_L\, \dot{\gamma}_{nt} = \mu_L \sqrt{\left(\frac{\partial \tilde{u}_x}{\partial \tilde{y}} + \frac{\partial \tilde{u}_y}{\partial \tilde{x}}\right)^2 + \left(\frac{\partial \tilde{u}_x}{\partial \tilde{z}} + \frac{\partial \tilde{u}_z}{\partial \tilde{x}}\right)^2} \tag{4}$$

where $\tilde{x}$, $\tilde{y}$, and $\tilde{z}$ represent co-ordinates of local co-ordinate systems aligned in flow direction, $\tilde{u}_i$ are local velocities, and μ_L is the laminar (dynamic) viscosity. Detailed explanations of the mathematical models can be found elsewhere [15, 16].

2.3 Particle Image Velocimetry

A cuboidal Plexiglas™ model of the DynaDrive BPC was built for the PIV experiments. The tank was filled with 50 L of water and rhodamine B coated poly(methyl methacrylate) fluorescent particles (20–50 μm) were added. A double-pulse 532 nm Nd:YAG laser (Bernoulli 145-15 PIV, Litron Lasers Ltd) with a sheet optics system was used to generate planar laser fields required for the 2D PIV. A highly sensitive 14-bit charge-coupled device (CCD) camera (Imager Pro X 4M, LaVision GmbH) was positioned perpendicular to the laser field and a 50 mm fixed focal length lens from Nikon was used. Using an external trigger device (WL12L-2B530 Laser, Sick AG) installed on the agitator shaft a fixed impeller position was captured in each frame. The DaVis 10 FlowMaster software (LaVision GmbH) was used for image acquisition and post-processing.

2.4 Cell Cultures, Media, and Virus Material

The Gibco™ ExpiSf9™ cells were maintained in Gibco™ ExpiSf™ CD medium throughout the seed train and bioreactor cultures. After thawing, the cells were incubated in Erlenmeyer flasks and sub-cultivated in Fernbach flasks with volumes of up to 1 L. The cultures were agitated at 125 rpm and 25 mm in a humidified incubator (Thermo Scientific™, Large-Capacity Reach-In CO$_2$ Incubator) at 27 °C. The ExpiSf9 cells were seeded with a cell density of ~0.9×10^6 cells mL^{-1} and sub-cultivated after three or four days with a maximum cell density of 8×10^6 cells mL^{-1}. The initial volumes in the two bioreactors were 1.0 L and 15 L for the benchtop and pilot scale respectively. The dissolved oxygen concentration was controlled at 40 %sat. Pure oxygen was sparged through the drilled hole sparger with a maximum flow rate of 0.1 vvm based on the DO control, whereas a constant air flow rate of 0.05 vvm was used for the headspace. The culture's pH value was monitored only and not controlled.

On the day prior to infection, the cells were diluted 1:1 with a target cell density of 3×10^6 cells mL^{-1} and the ExpiSF enhancer (Gibco™ ExpiSf™ Protein Production Kit, Cat. No. A3767808) was added at a volume of 4 mL L^{-1}. The cells were infected with a multiplicity of infection (MOI) of 2 using two baculoviruses that contain the RepCap2 and inverted terminal repeat green fluorescent protein (IRT-GFP) with virus titers of 2.2×10^9 vg mL^{-1} and 1.9×10^9 vg mL^{-1} respectively. The RepCap2 baculovirus supplied the necessary viral genes for genome replication, genome packaging, and capsid assembly. The ITR–GFP baculovirus contained the gene of interest (encoding GFP) flanked by AAV ITR sequences.

2.6 Sampling and Analytics

Samples (~10 mL) from the bioreactors were taken daily. Substrate and metabolite concentrations were analyzed using the BioProfile™ Flex-2™ bioanalyzer (Nova Biomedical). The viable and total cell density, the viability, and the cell diameter were determined using the Vi-CELL™ XR cell analyzer (Beckman Coulter). The offline pH value was measured using the pH 150 meter (Oakton), and it was used to re-calibrate the pH probes in the glass bioreactor and DynaDrive S.U.B. if the pH value differed by more than 0.1 pH units from the online value.

After the virus infection, five 1 mL aliquots were frozen for the virus titer analyses. For determination of rAAV viral genome titers, quantitative PCR (qPCR) was adopted using GFP-specific primers and a GFP-specific probe that target the gene of interest flanked by the ITR sequences of the packaged viral DNA. Prior to qPCR analysis, non-encapsulated DNA was removed from crude lysates by DNase I treatment and encapsulated AAV genomes were released from AAV particles by treatment with Proteinase K. qPCR was performed on an Applied Biosystems™ QuantStudio™ 7 Flex Real-Time PCR System, and rAAV titers were determined based on a standard curve of linearized GFP-containing plasmid.

3 Results

3.1 Flow in the DynaDrive 50 L S.U.B.

The flow in the single-use bioreactor was simulated for three working volumes (15 L, 30 L, and 50 L) in this study, but only results for the two lower volumes used in the experiments are shown in Fig. 2. In agreement with expectations, the CFD model revealed a predominantly axial discharge from the marine impellers. For a counter-clockwise rotation, the liquid was pumped downwards towards the vessel bottom where it was transported outwards towards the vertical walls. The liquid then flowed upwards before re-entering the impeller zones. Due to the off-centered
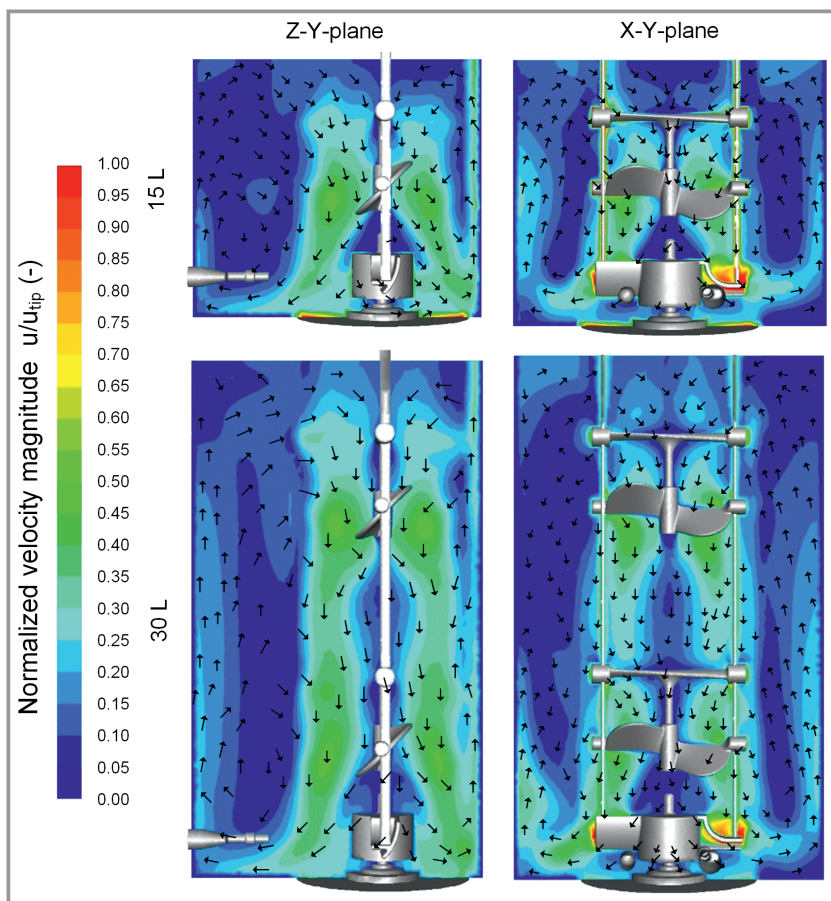
Figure 2. CFD predicted flow patterns in the DynaDrive 50-L bioreactor with 15 L and 30 L working volumes.

location of the impeller, the size of the loop was asymmetrical in the two vessel halves. As expected, the maximum velocities were close to the impeller tip speeds ($u_{tip} = \pi N_R d_R$). Velocities between 0.2 and 0.6 u_{tip} were found for the majority of the bulk region, whereas lower velocities where predicted close to the top and bottom corners as well as in the center of the flow loops. However, no stagnant regions were identified.

Results of the particle image velocimetry experiments are depicted in Fig. 3a. The color bars were mapped to the agitator tip speed ($0.7 \, \text{m s}^{-1}$) represented by the dark red color, whereas the dark blue color represents the lowest measured fluid velocities ($\sim 0 \, \text{m s}^{-1}$). The vectors indicate the local flow direction within the measurement plane, but they do not include the velocity component perpendicular to the measurement plane. Consequently, the effective fluid flow may be in a different direction. Several large areas of high velocities ($> 0.7 \, \text{m s}^{-1}$) were found in the vicinity of the impeller elements as well as near the tank bottom. These were most likely caused by optical distortions, reflections from the plastic tank, and/or false cross correlations in the PIV data post processing. The latter can be caused by very small or large displacements of the fluorescence particles

between the double frames or by non-uniform particle image intensities [17–19].

Despite these artifacts, the particle image velocimetry measurements confirmed the expected and CFD predicted flow pattern. The highest velocities were measured close to the impeller tips, and they agreed well with the agitator tip speed. Velocities of approx. 0.25 to 0.5 u_{tip} were determined in the swept volume of the agitator, whereas much lower velocities were found predominantly in the rest of the tank. The PIV measurements also confirmed the down-pumping flow through the marine impellers and the upwards flow along the vessel walls. Comparing the CFD predictions with the measurements, the axial flow seemed to be over-predicted in the simulations, but main features of the flow pattern were correctly captured.

A more quantitative comparison between the CFD model and the PIV results was difficult because of the torsion of the agitator ropes which resulted in a misalignment of the impellers, as shown in Fig. 3b. Consequently, the mid-impeller planes were rotated relative to the vessel planes which was not considered in the CFD models. It was also found that this misalignment was different between the impeller stages and dependent on the rotational speed and filling volume. In order to improve the agreement of the CFD simulations and the PIV measurements, the measured torsion could be considered during the CFD mesh generation, but this was beyond the scope of this study.

3.2 Comparison of the DynaDrive and Glass Bioreactor Flow Data

In order to compare the small- and large-scale bioreactors, the volume frequency distributions for the velocity magnitude as well as the radial, axial, and tangential velocity components were determined, as shown in Fig. 4. The velocities were normalized by the impeller tip speeds and discretized into 50 classes. The distributions were found to be independent of the agitator speed (i.e., self-similar), which agreed with expectations. The y-axes represent the volume fraction of fluid domain where a specific velocity occurs. For instance, velocities between 0.21 u_{tip} and 0.23 u_{tip} occurred in 14 % of the whole volume in the glass bioreactor. Assuming that the cell density is homogeneous and that the cells follow the fluid flow, the volume frequency distributions
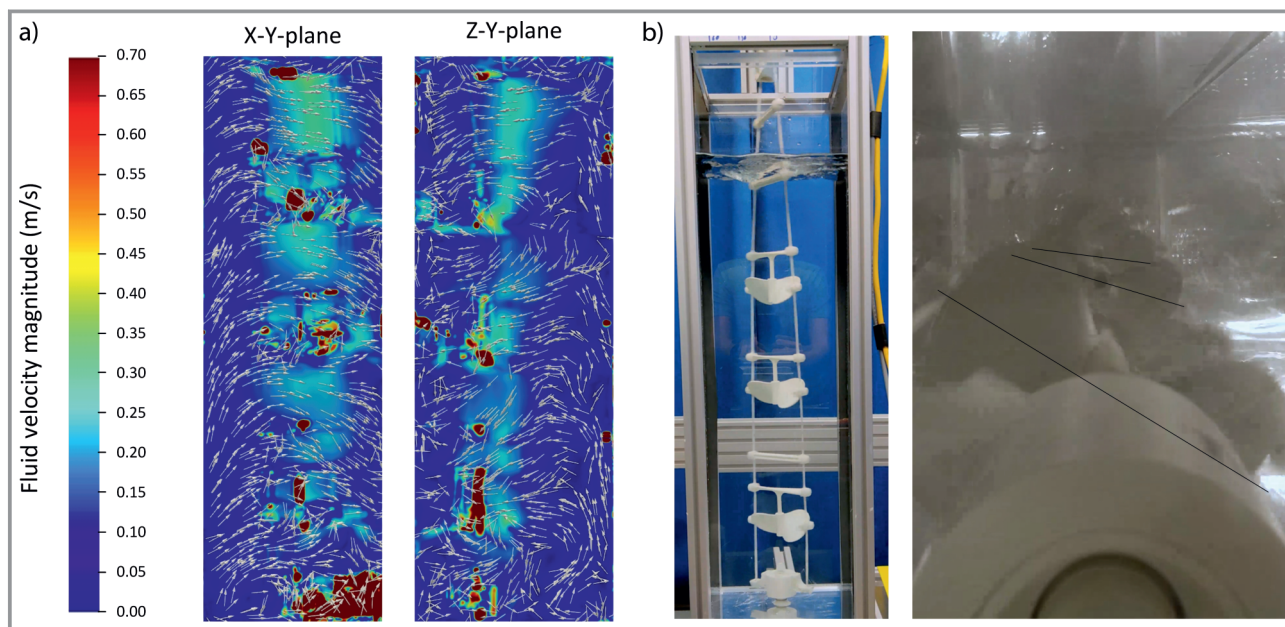
Figure 3. 2D-PIV results for the two mid-vessel planes of the DynaDrive bioreactor with 50 L working volume agitated at 100 rpm (a) and picture of the agitator during rotation taken from the front and bottom of the vessel (b). The black lines on the right side indicate the impeller axes identified by video capturing.

can be considered as residence time distributions. This means that the cells are exposed to above-mentioned fluid velocities (and resulting shear stresses) over 14 % of the total process time, for instance.

The distributions for the axial velocities were very similar between the two bioreactors, but larger differences were found for the radial and tangential velocity components as well as for the velocity magnitude. The peak for these
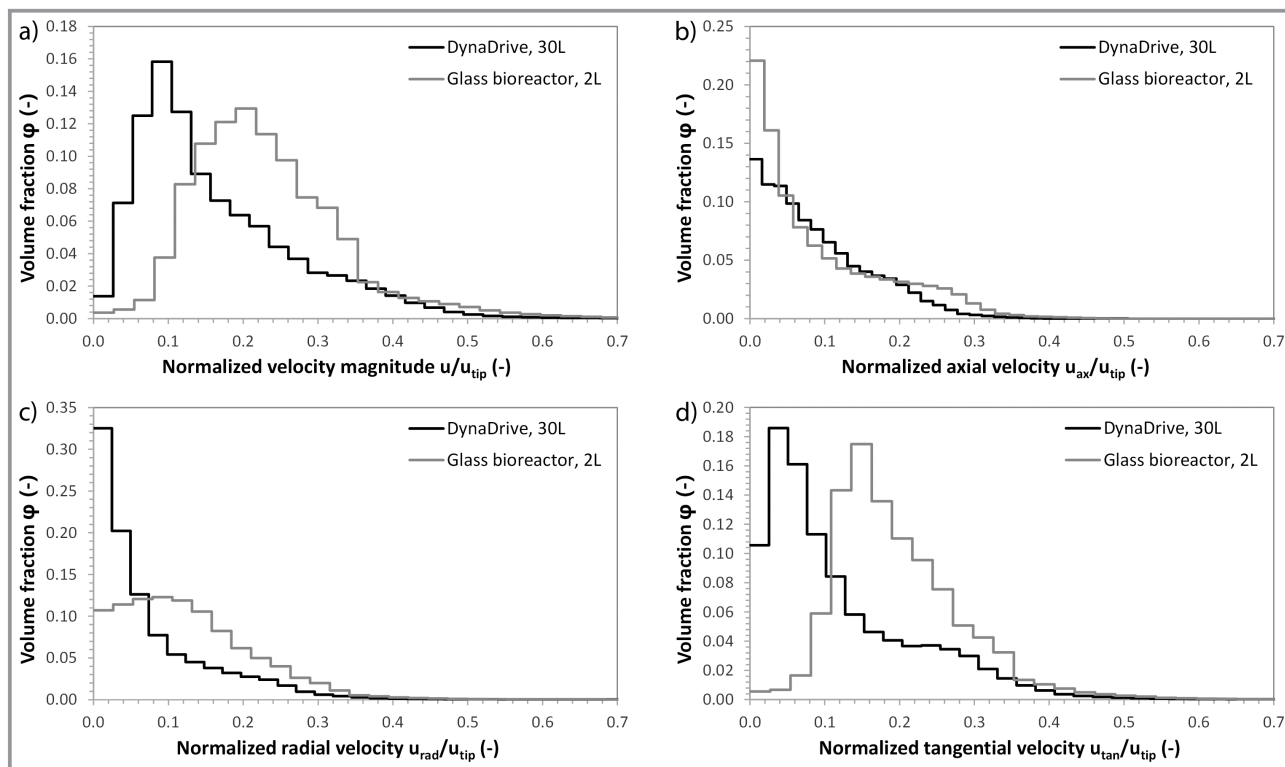

Figure 4. Normalized velocity distributions for the two bioreactors with maximum working volume. a) Velocity magnitude, b) axial velocity, c) radial velocity, and d) tangential velocity.

distributions were shifted towards smaller velocities in the DynaDrive S.U.B. For instance, velocities of ~0.1 u_{tip} occurred in 16 % of the DynaDrive S.U.B. volume but only in 4 % of the glass bioreactor whereas the glass bioreactor's peak volume fraction was found for ~0.2 u_{tip}. The weaker radial velocities in the DynaDrive S.U.B. can be explained by the predominantly axial discharge of the marine impellers inside the single-use bioreactor. The lower tangential velocities could be a result of the rectangular tank and the off-centered agitator position. Both attributes are known to reduce vortex formation and improve mixing [20].

3.3 Engineering Data

Distinct profiles for the power numbers were obtained (Fig. 5), but interestingly the power numbers for the two bioreactors were similar when one or two impellers were submerged. Power numbers in the range of 1.8 and 2.0 were found for the lowest working volume, whereas the power numbers were in the range of 2.7 and 3.3 with two impellers submerged. The DynaDrive S.U.B. had a power number of approximately 3.74 for the maximum volume. In agreement with experimental data [21], the power numbers for the glass bioreactor decreased with increasing Reynolds numbers which can be explained by the absence of baffles. The power numbers in the DynaDrive S.U.B. were almost independent of the Reynolds number which indicates fully turbulent conditions above Reynolds numbers of 10^4. No experimental data were available for validation.

Fig. 6 shows the CFD predicted mixing times for both bioreactors, and experimental data obtained with the conductivity method is also given. As expected, the simulated mixing times decreased for both bioreactors with increasing power input. The mixing times in the glass bioreactor were in the range of 5 s and 17 s, whereas the DynaDrive S.U.B. had mixing times in the range of 6 s and 90 s. It should be noted that the experimental data for the glass bioreactors
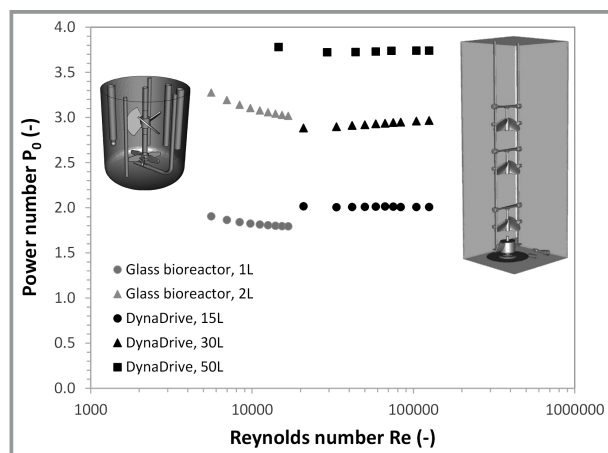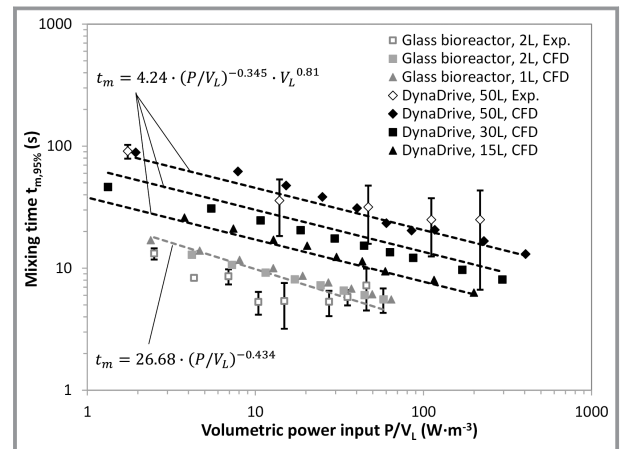

Figure 6. CFD-predicted and experimental mixing times in both bioreactors. The dashed lines represent the regression functions.

was noticeably lower than the CFD predictions for most conditions. This can be explained by the locally measured conductivity in the experiments, whereas the CFD simulations capture the entire fluid volume. However, better agreement was found for the DynaDrive S.U.B. with 50 L working volume.

The volume averaged fluid stresses, expressed as shear and normal stresses based on Eqs. (3) and (4), are plotted as a function of the volumetric power inputs in Fig. 7. As expected, the normal stresses were smaller than the shear stresses with values in the range of 0.92×10^{-3} N m^{-2} and 7.4×10^{-3} N m^{-2}. Interestingly, all data points could be expressed by a single correlation regardless of the bioreactor and filling volume (solid line in Fig. 7). In contrast, two distinct profiles were found for the shear stresses in the glass bioreactor and the DynaDrive S.U.B. respectively. The shear stresses increased with increasing power inputs from 2.2×10^{-3} N m^{-2} to 21.4×10^{-3} N m^{-2} in the DynaDrive S.U.B. and from 4×10^{-3} N m^{-2} to 20.5×10^{-3} N m^{-2} in the glass

Figure 5. CFD-predicted power numbers as a function of Reynolds number for the two bioreactors with minimum and maximum working volumes used in this study.
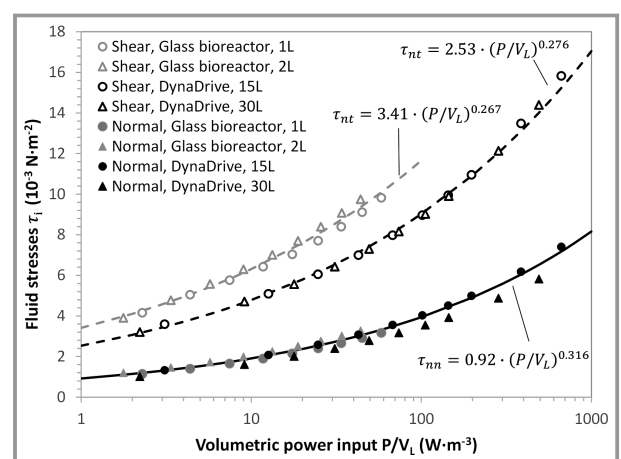

Figure 7. CFD-predicted shear and normal stresses in the two bioreactors.

bioreactor. Though, it should be emphasized that volumetric power inputs in cell cultures usually do not exceed $100\,\mathrm{W\,m^{-3}}$ [22].

3.4 Cell Culture Performance

The profiles for the cell density and viability are shown in Fig. 8. Good agreement was found between the two runs for each bioreactor, with relative deviations of 12 % or less for most data points, which indicates the good reproducibility of the results. The viable cell density increased exponentially in all bioreactors and reached concentrations between $5.89\times10^6\,\mathrm{cells\,mL^{-1}}$ (DynaDrive S.U.B., run#2) and $7.38\times10^6\,\mathrm{cells\,mL^{-1}}$ (Glass bioreactor, run#2) within 72 h. This corresponds to growth rates between $0.66\,\mathrm{d^{-1}}$ and $0.72\,\mathrm{d^{-1}}$ and doubling times of 25.3 h and 23.1 h respectively. In agreement with expectations, only minor cell growth was observed after the media and enhancer addition (after 96 h). The highest concentrations of the infected cells were observed one day after the virus addition with values between $4.19\times10^6\,\mathrm{cells\,mL^{-1}}$ (DynaDrive S.U.B., run#2) and $6.22\times10^6\,\mathrm{cells\,mL^{-1}}$ (glass bioreactor, run#1). Afterwards, the viable cell density decreased due to the progressive cell death and lysis. This can also be seen in the cell viability which dropped dramatically from $>95\,\%$ after 120 h to $<50\,\%$ at the end of the process.

The virus amplification could also be monitored via the increase in cell diameter, as shown Fig. 9a. The uninfected cells had cell diameters of $\sim15.5\,\mu\mathrm{m}$, but the diameter of the infected cells increased up to $17.7\,\mu\mathrm{m}$ (DynaDrive S.U.B.) and $18.1\,\mu\mathrm{m}$ (glass bioreactor) after 144 h, i.e., two days post infection (p.I.). Afterwards, the cell diameter

dropped again which can be explained by the decrease in cell viability and formation of cell debris in the culture broth.

Profiles of the substrate glucose and the ammonia concentration, which were also very consistent across the two runs in the two bioreactors, are shown in Figs. 9b and c respectively. The decrease in the glucose concentration prior to and post infection can be attributed to the metabolism resulting from cell growth and the virus production. Interestingly, the glucose concentration was lowest in all samples of the glass bioreactor in run1 after the virus addition with an offset of $\sim1.0\,\mathrm{g\,L^{-1}}$ relative to the other samples for both runs. It should be noted that different media bags were used for the two batches. However, no glucose limitations were expected at any point in time. The ammonia concentration decreased from $>1\,\mathrm{g\,L^{-1}}$ to $<0.2\,\mathrm{g\,L^{-1}}$ during the exponential growth phase and after the media addition, whereas it increased towards the end of the process. This may be explained by cell lysis and the resulting release of cell plasma into the culture media.

Finally, the obtained virus titers are summarized in Fig. 9d. The results of the glass bioreactor agreed well with the historical data obtained in the 3-L glass bioreactor (reference), and they were very consistent between the two runs resulting in standard deviations of below 10 %. The highest virus titers of $1.66\times10^{11}\,\mathrm{vg\,mL^{-1}}$ (run#1) and $1.69\times10^{11}\,\mathrm{vg\,mL^{-1}}$ (run#2) were achieved two and three days p.I. respectively, whereas the virus concentration decreased slightly on day 4. The DynaDrive bioreactor showed slightly higher variations between the two runs, but the results were still within expected ranges. The peak titers in the DynaDrive bioreactor were $1.59\times10^{11}\,\mathrm{vg\,mL^{-1}}$ three days p.I. (run#1) and $1.13\times10^{11}\,\mathrm{vg\,mL^{-1}}$ four days p.I. (run#2) respectively. These differences can be explained by the fact that different cell thaws and seed viruses were used for the two batches. Furthermore, the titers were quantified on different qPCR plates. The maximum titers in the DynaDrive S.U.B. were comparable with those achieved in the reference in both runs. It should be noted that the greenish color from the GFP protein was visible to the naked eye in both bioreactors, but it was more pronounced in the DynaDrive S.U.B. bioreactor.
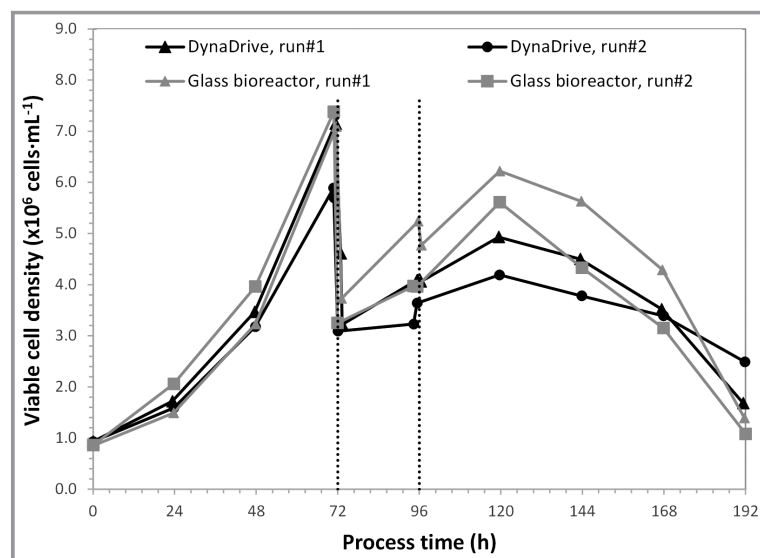
4 Discussion

Various studies have demonstrated that CFD can be used to characterize and compare the flow of geometrically similar or non-similar bioreactors at different scales in detail [10, 23, 24]. While CFD provides local flow data, volume-averaged parameters, such as power inputs, mixing times and oxygen mass transfer rates, are still pre-dominantly used for scaling up of cell
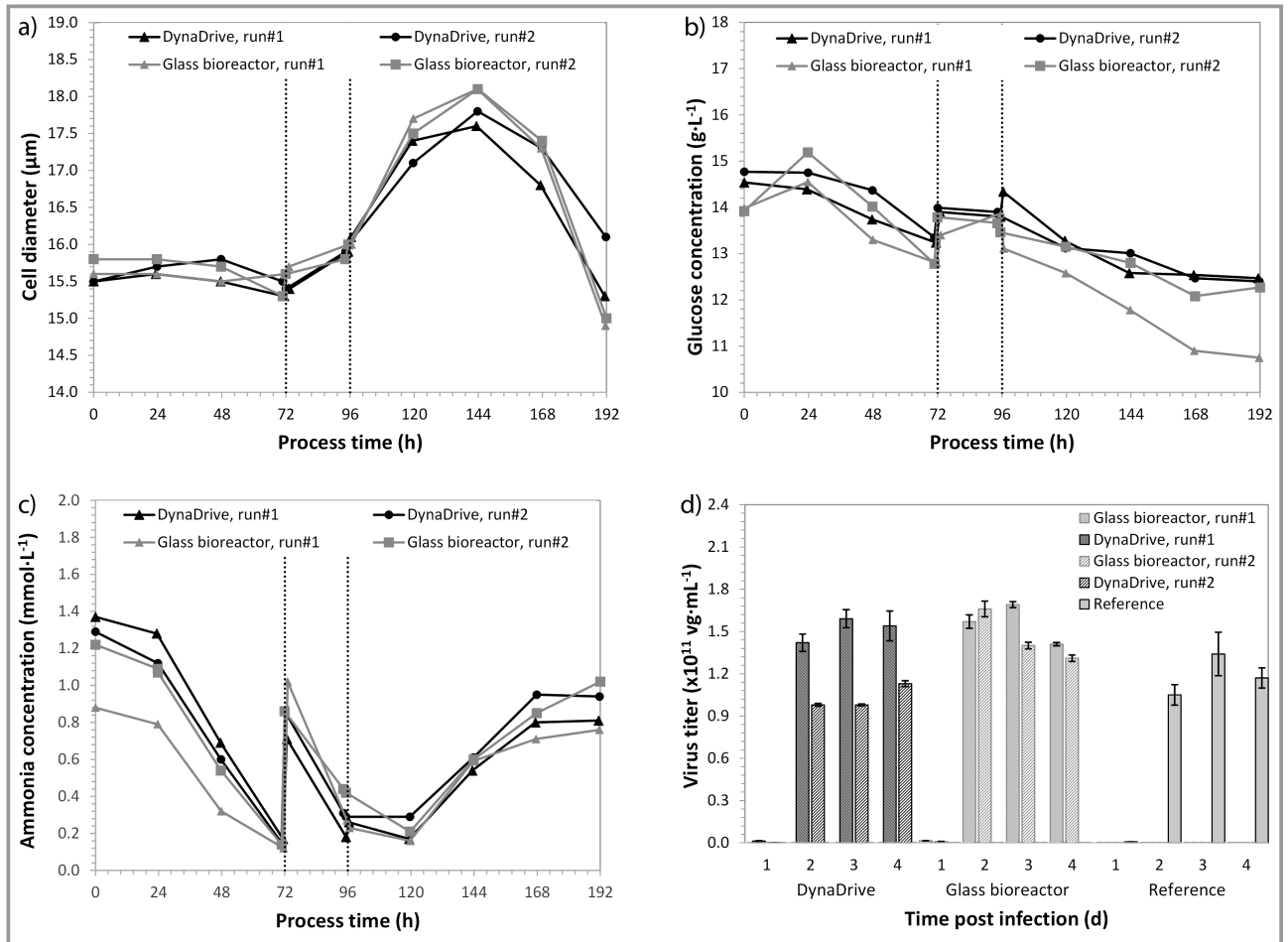

Figure 8. Profiles of the viable cell density and viability in the two bioreactors. The dashed indicate the addition of cell culture media after 72 h and the virus infection after 96 h respectively.

Figure 9. Profiles of the cell diameter (a), glucose concentration (b), ammonia concentration (c), and the virus titer (d) in the two bioreactors. The dashed indicate the addition of cell culture media after 72 h and the virus infection after 96 h respectively. Historical data for the virus titer is shown in Fig. 9d for reference.

cultures for practical reasons. In the present case, engineering data for the DynaDrive S.U.B. were predicted by CFD due to the lack of experimental data. Based on preliminary small-scale experiments, optimal virus titers were achieved using volumetric power inputs of ~35 W m⁻³ (Tab. 3).

It was found that at this power input very short mixing times of less than 10 s can be achieved in the benchtop scale bioreactor. It has been shown that a CHO cell culture had an optimum cell growth at approximately 12 s in benchtop agitator bioreactors whereas both less and more mixing

Table 3. Summary of engineering data and scale-up parameters related to the agitation in the two bioreactors.

System	Impeller speed [rpm]	Tip speed [m s⁻¹]	Reynolds number [–]	Volumetric power [W m⁻³]	Power number [–]	Mixing time [s]	Volume averaged stresses [10⁻³ N m⁻²]	
							τ_{nn}	τ_{nt}
HyPerforma Glass bioreactor								
1.0 L	200	0.565	13 966	33.8	1.80	5.8	2.7	8.4
2.0 L	220	0.622	15 363	34.0	3.03	5.8	3.0	9.1
DynaDrive S.U.B.								
15 L	112	0.776	46 870	35.0	2.01	11.1	2.8	6.8
30 L	125	0.863	52 082	35.0	2.93	19.1	2.8	6.8

resulted in lower cell growth [25]. Though, no similar investigations with insect cells were found in the literature. Based on the obtained mixing times and previous findings for CHO cells [25], no mixing limitations were expected both at benchtop and pilot scale. However, it should be noted that, similar to previous studies [23], the mixing time was no suitable scale-up criterion in our case. In order to achieve similar mixing times at both scales, the volumetric power input would exceed $100 \, W \, m^{-3}$ and could result in excessive mechanical stress of the insect cells. Furthermore, it is known that infected insect cells are more sensitive to shear stresses than non-infected insect cells.

The CFD predicted volume-averaged shear stresses at moderate agitation were $8.4 \times 10^{-3} \, N \, m^{-2}$ and $9.1 \times 10^{-3} \, N \, m^{-2}$ for the two working volumes respectively. Using small-scale stirred bioreactors (0.5 L working volume) it has been found that measles virus titers produced by Vero cells growing on a Cytodex™ microcarriers are sensitive to agitator-dependent shear, with shear stresses $\geq 250 \times 10^{-3} \, N \, m^{-2}$ reducing the titer by more than four orders of magnitude [26]. Adherent growing Vero cells were found to tolerate maximum shear stress levels in the range 3.5 to 5 $N \, m^{-2}$, depending on the cultivation device and cultivation conditions [26–28]. This is several orders of magnitude higher than the volume-averaged stresses found here. Other studies found that sublethal cell damage and cell death started to occur in the range of shear stresses from 0.5–200 $N \, m^{-2}$ [29]. The wide range resulted from differences in cell lines, culture media and shear conditions, including the exposure time. At the larger scale, shear stresses of $6.8 \times 10^{-3} \, N \, m^{-2}$ were predicted at the same power input. Therefore, it can be concluded that the expected hydrodynamic stresses in the DynaDrive S.U.B. were non-critical.

As can also be seen from Tab. 3, the Reynolds number in the DynaDrive S.U.B. was about fivefold the Reynolds numbers in the glass bioreactor due to the larger impellers ($Re \propto d_R{}^2$). Therefore, fully turbulent conditions could be expected in the large-scale system. Hence, when maintaining a similar volumetric power input between the scales, turbulent mixing could be expected in both bioreactors.

In addition to the agitation, the aeration in the DynaDrive bioreactor had to be scaled-up. The oxygen mass transfer coefficient or mass transfer rate is often used as a scale-up parameter. However, the oxygen mass transfer was not predicted based on the CFD models in this study predominantly for two reasons:

a) Two-phase models are required to predict the gas distribution, (local) gas hold-ups, and bubble surface area which usually include sub-models for gas-liquid turbulence, bubble coalescence and bubble breakup as well as special boundary conditions for the inlet bubble size distribution [30]. No experimental data were available to set these boundary conditions and/or validate the results in the present study.

b) The computational effort of two-phase simulations, which are usually transient, exceeds those of steady-state

single-phase simulations by one or two orders of magnitude. For example, a two-phase simulation using the sliding mesh approach took 14 d whereas the single-phase mixing simulation took only a few hours on a multi-threaded workstation. Similar turnaround times have been reported in the literature [9].

Even though an increasing number of publications on multi-phase CFD simulations became available over the last two decades [9, 10, 30–33], their practical use for scale-up studies on bioreactors is still limited, especially when the required boundary conditions and model closures are unknown. Consequently, it was decided to maintain the maximum volumetric gas flow rate (in vvm) between the systems while using pure oxygen sparging for DO control, as proposed for a monoclonal antibody production process [34]. Based on the oxygen demands of the cultures and the PID settings of the controllers, the effective gas flow rates were significantly lower while maintaining the desired DO level of 40 % sat in both bioreactor systems. Considering experimental data, oxygen mass transfer rates of up to 10 mmol L^{-1} were expected in the DynaDrive S.U.B. which was about five-fold higher than those achievable in the glass bioreactor at similar agitation. This can be explained by the more effective sparger system in the DynaDrive S.U.B. which has significantly smaller hole sizes resulting in smaller initial bubbles (see Tab. 1). Therefore, no oxygen limitation was expected for cell densities of up to 25×10^6 cells mL^{-1} based on reported specific oxygen consumption rates for Sf9 cells in the range of 2.2 to 3.82×10^{-13} mol h^{-1}cell^{-1} [30, 35, 36].

Based on the growth, substrate consumption and virus titer profiles, the culture was successfully scaled-up from the benchtop to two-digit liter range. It can be seen from Tab. 4 that the achieved titers, yields, and virus productivity were comparable between the two scales even though further optimization is required. To the best of the author's knowledge, this was the first successful scale-up of an AAV production using the ExpiSf Expression system in conjunction with a pilot scale single-use bioreactor. It should be noted that the DynaDrive S.U.B. has a higher maximum capacity of up to 50 L. However, this volume was beyond the scope of this study and will be addressed in future research.

5 Conclusions

The current study clearly demonstrates the scalability of the ExpiSf Expression system for recombinant AAV production from the benchtop to the two-digit liter scale. A 15-fold increase in volume was achieved expanding the capacities of the recombinant AAV production considerably. The pilot bioreactor yielded between 3.3 and 4.8×10^{15} vg that, depending on the therapy, can be sufficient for the treatment of a single patient. Furthermore, it was demonstrated that the ExpiSf Expression System itself is a scalable option for

Table 4. Summary of process characteristics for the virus production process in the two bioreactors.

Bioreactor	Glass bioreactor ($n = 2$)	DynaDrive bioreactor ($n = 2$)
Peak cell density [10^6 cells mL^{-1}]	7.24 ± 0.21	6.52 ± 0.89
Peak virus titer [10^{11} vg mL^{-1}]	1.68 ± 0.02	1.36 ± 0.33
Final viability [%]	19.5 ± 1.1	38.8 ± 11.2
Yield glucose[a)] [10^9 cells gGluc^{-1}]	2.98 ± 0.31	4.14 ± 0.91
Yield AAV [10^2 vg cell^{-1}]	1.11 ± 0.1	0.69 ± 0.33
Productivity [10^{11} vg mL^{-1} h^{-1}]	0.021 ± 0.003	0.014 ± 0.003

[a)] Determined during the exponential cell growth.

baculovirus processes for research use, allowing for comparably high titers that are typically seen in glass bioreactors. In addition to the virus expression investigated in the present study, a scalable production of recombinant AAV for gene therapy applications seems conceivable. Further process optimization as well as increase in volume to 50 L using the full capacity of the DynaDrive single-use bioreactor will be part of future studies.

Symbols used

d_R	[m]	impeller diameter
M	[Nm]	impeller torque
N_R	[s^{-1}]	impeller rotational speed
P	[W]	power input
P_0	[–]	power number
Re	[–]	Reynolds number
$\tilde{u}_i$	[m s^{-1}]	fluid density in local co-ordinates
U	[m s^{-1}]	fluid velocity
u_{tip}	[m s^{-1}]	impeller tip speed
V_L	[m^3]	liquid volume
$\tilde{x}, \tilde{y}, \tilde{z}$	[m]	local co-ordinates

Greek letters

$\dot{\gamma}_{nn}$	[s^{-1}]	normal velocity gradient
$\dot{\gamma}_{nt}$	[s^{-1}]	shear velocity gradient
ρ_L	[kg m^{-3}]	fluid density
μ_L	[Pa s]	laminar (dynamic) viscosity
τ_{nn}	[N m^{-2}]	normal stress
τ_{nt}	[N m^{-2}]	shear stress
φ	[–]	volume fraction

Abbreviations

AAV	adeno associated virus
BPC	bioprocess container
CCD	charge-coupled device
CD	chemically defined
CFD	computational fluid dynamics
DHS	drilled hole sparger
DO	dissolved oxygen
GFP	green fluorescent protein
IRT	inverted terminal repeat
MOI	multiplicity of infection
MRF	multiple reference frame
PIV	particle image velocimetry
PCR	polymerase chain reaction
RTD	resistance temperature device
Sf9	*Spodoptera frugiperda*, subclone 9
SM	sliding mesh
SUB	single-use bioreactor

References

[1] *Markets and Markets 2020, Protein expression market global forecast to 2025 by type, products, application, end user*, Thermo Fisher market analysis, internal report **2020**.

[2] J. Fuenmayor, F. Gòdia, L. Cervera, *New Biotechnol.* **2017**, *39*, 174–180. DOI: https://doi.org/10.1016/j.nbt.2017.07.010

[3] E. Puente-Massaguer, F. Gòdia, M. Lecina, *J. Biotechnol.* **2020**, *322*, 43–53. DOI: https://doi.org/10.1016/j.jbiotec.2020.07.009

[4] L. Käßer, J. Harnischfeger, D. Salzig, P. Czermak, *Electron. J. Biotechnol.* **2022**, *56*, 54–64. DOI: https://doi.org/10.1016/j.ejbt.2022.01.004

[5] J. H. Kurasawa, A. Park, C. R. Sowers, R. A. Halpin, A. Tovchigrechko, C. L. Dobson, A. E. Schmelzer, C. Gao, S. D. Wilson, Y. Ikeda, *Mol. Ther. Methods Clin. Dev.* **2020**, *19*, 330–340. DOI: https://doi.org/10.1016/j.omtm.2020.09.018

[6] https://assets.thermofisher.com/TFS-Assets/BPD/Application-Notes/process-performance-comparison-50l-hyperforma-dynadrive-sub-legacy-subs.pdf (Accessed on September 20, 2022).

[7] https://bioprocessintl.com/sponsored-content/bioprocess-selection-and-economics-5000-l-dynadrive-bioreactor-shifting-the-paradigm/ (Accessed on September 20, 2022).

[8] S. Kaiser, V. Jossen, C. Schirmaier, D. Eibl, S. Brill, C. van den Bos, R. Eibl, *Chem. Ing. Tech.* **2013**, *85 (1–2)*, 95–102. DOI: https://doi.org/10.1002/cite.201200180

[9] D. Kreitmayer, S. R. Gopireddy, T. Matsuura, Y. Aki, Y. Katayama, H. Kakihara, K. Nonaka, T. Profitlich, N. A. Urbanetz, E. Gutheil, *Biochemic. Eng. J.* **2022**, *177*, 108237. DOI: https://doi.org/10.1016/j.bej.2021.108237

[10] J. Scully, L. B. Considine, M. T. Smith, E. McAlea, N. Jones, E. O'Connell, E. Madsen, M. Power, P. Mellors, J. Crowley, N. O'Leary, S. Carver, D. Van Plew, *Biotechnol. Bioeng.* **2022**, *117 (6)*, 1710–1723. DOI: https://doi.org/10.1002/bit.27323

[11] http://assets.thermofisher.com/TFS-Assets/BID/Application-Notes/scalable-aav-vector-production-purification-expisf-expression-system-app-note.pdf (Accessed on September 22, 2022).

[12] https://assets.thermofisher.com/TFS-Assets/BPD/brochures/dynadrive-sub-brochure.pdf (Accessed on May 17, 2022).

[13] https://assets.thermofisher.com/TFS-Assets/BPD/Datasheets/50l-dynadrive-sub-data-sheet.pdf (Accessed on May 17, 2022).

[14] https://www.scribd.com/document/472950167/ANSYS-Fluent-Users-Guide-v19-2-by-ANSYS-z-lib-org-pdf (Accessed on May 17, 2022).

[15] S. Wollny, *Experimentelle und numerische Untersuchungen zur Partikelbeanspruchung in gerührten (Bio-)Reaktoren*, Ph.D. Thesis, Technische Universität Berlin **2010**.

[16] B. Krause, in *Tagungsband 10. Köthener Rührerkolloquium* (Ed: R. Sperling), Köthener Rührerkolloquium, Köthen **2007**.

[17] J. Rohaly, T. Nakajima, Y. Ikeda, *Exp. Fluids* **2000**, *29 (7)*, S023–S033. DOI: https://doi.org/10.1007/s003480070004

[18] J. Nogueira, A. Lecuona, P. A. Rodriguez, *Meas. Sci. Technol.* **1997**, 8, 1493–1501. DOI: https://doi.org/10.1088/0957-0233/8/12/012

[19] A. Sciacchitano, B. Wieneke, F. Scarano, *Meas. Sci. Technol.* **2013**, *24 (4)*, 045302. DOI: https://doi.org/10.1088/0957-0233/24/4/045302

[20] F. Liepe, R. Sperling, S. Jembere, *Rührwerke: theoretische Grundlagen, Auslegung und Bewertung*, Fachhochschule Köthen Eigenverlag, Köthen **1999**.

[21] S. C. Kaiser, S. Werner, V. Jossen, M. Kraume, D. Eibl, *Eng. Life Sci.* **2017**, *17 (5)*, 500–511. DOI: https://doi.org/10.1002/elsc.201600096

[22] A. W. Nienow, *J. Chem. Eng. Jpn.* **2009**, *42 (11)*, 789–796. DOI: https://doi.org/10.1252/jcej.08we317

[23] S. C. Kaiser, C. Löffelholz, S. Werner, D. Eibl, in *Computational Fluid Dynamics Technologies and Applications* (Eds: I. V. Minin, O. V. Minin), InTech, London **2011**. DOI: https://doi.org/10.5772/23496

[24] S. Werner, J. Olownia, D. Egger, D. Eibl, *Chem. Ing. Tech.* **2013**, *85 (1–2)*, 118–126. DOI: https://doi.org/10.1002/cite.201200153

[25] O. Platas Barradas, U. Jandt, L. Da Minh Phan, M. E. Villanueva, M. Schaletzky, A. Rath, S. Freund, U. Reichl, E. Skerhutt, S. Scholz, T. Noll, V. Sandig, R. Pörtner, A.-P. Zeng, *Eng. Life Sci.* **2012**, *12 (5)*, 518–528. DOI: https://doi.org/10.1002/elsc.201100163

[26] T. A. Grein, D. Loewe, H. Dieken, T. Weidner, D. Salzig, P. Czermak, *Front. Bioeng. Biotechnol.* **2019**, 7, 78. DOI: https://doi.org/10.3389/fbioe.2019.00078

[27] M. Hjortso, *Cell Adhesion in Bioprocessing and Biotechnology*, Taylor and Francis, New York **1994**.

[28] C. F. Crouch, H. W. Fowler, R. E. Spier, *J. Chem. Technol. Biotechnol.* **1995**, *35*, 273–281. DOI: https://doi.org/10.1002/jctb.280350408

[29] L. van der Pol, J. Tramper, *Trends Biotechnol.* **1998**, *16 (8)*, 323–328. DOI: https://doi.org/10.1016/S0167-7799S

[30] S. Seidel, R. W. Maschke, S. Werner, V. Jossen, D. Eibl, *Chem. Ing. Tech.* **2021**, *93 (1–2)*, 42–61. DOI: https://doi.org/10.1002/cite.202000179

[31] F. Kerdouss, A. Bannari, P. Proulx, R. Bannari, M. Skrga, Y. Labrecque, *Comp. Chem. Eng.* **2008**, *32*, 1943–1955. DOI: https://doi.org/10.1016/j.compchemeng.2007.10.010

[32] J. Sarkar, L. Kanwar Shekhawat, V. Loomba, A. S. Rathore, *Biotechnol. Prog.* **2016**, *32 (2)*, 613–628. DOI: https://doi.org/10.1002/btpr.2242

[33] S. Seidel, D. Eibl, *Processes* **2021**, 9, 1185. DOI: https://doi.org/10.3390/pr9071185

[34] S. Xu, L. Hoshan, R. Jiang, B. Gupta, E. Brodean, K. O'Neill, C. T. Seamans, J. Bowers, H. Chen, *Biotechnol. Prog.* **2017**, *33 (4)*, 1146–1159. DOI: https://doi.org/10.1002/btpr.2489

[35] L. A. Palomares, O. T. Ramirez, *Cytotechnology* **1996**, *22 (1–3)*, 225–237. DOI: https://doi.org/10.1007/BF00353943

[36] T. K. K. Wong, L. K. Nielsen, P. F. Greenfield, S. Reid, *Cytotechnology* **1994**, *15 (1–3)*, 157–167. DOI: https://doi.org/10.1007/BF00762390